2002

Landing Gear Aerodynamic Noise Prediction Using Unstructured Grids

Anupam Sharma, *Pennsylvania State University*
F. J. Souliez, *Pennsylvania State University*
L. N. Long, *Pennsylvania State University*
P.J. Morris, *Pennsylvania State University*

aeroacoustics volume 1 · number 2 · 2002 – pages 115 – 135

Landing gear aerodynamic noise prediction using unstructured grids

F.J. Souliez, L.N. Long, P.J. Morris and A. Sharma

Department of Aerospace Engineering, The Pennsylvania State University, University Park, PA 16802

ABSTRACT

Aerodynamic noise from a landing gear in a uniform flow is computed using the Ffowcs Williams-Hawkings (FW-H) equation. The time accurate flow data on the integration surface is obtained using a finite volume low-order flow solver on an unstructured grid. The Ffowcs Williams-Hawkings equation is solved using surface integrals over the landing gear surface and over a permeable surface away from the landing gear. Two geometric configurations are tested in order to assess the impact of two lateral struts on the sound level and directivity in the far-field. Predictions from the Ffowcs Williams-Hawkings code are compared with direct calculations by the flow solver at several observer locations inside the computational domain. The permeable Ffowcs Williams-Hawkings surface predictions match those of the flow solver in the near-field. Far-field noise calculations coincide for both integration surfaces. The increase in drag observed between the two landing gear configurations is reflected in the sound pressure level and directivity mainly in the streamwise direction.

NOMENCLATURE

c	speed of sound
D	wheel diameter
$H(f)$	Heaviside function, $H(f) = 0$ for $f < 0$ and $H(f) = 1$ for $f > 0$
L_i	refer to equation 2
$\mathbf{M}$	local Mach number vector of the source
M	$\lvert\mathbf{M}\rvert$
M_r	$M_i \hat{r}_i$
$\hat{n}$	unit normal vector to the surface
P_{ij}	compressive stress tensor
p	pressure
p_∞	freestream pressure
p'	total pressure fluctuation ($p - p_\infty$)
p_{RMS}	root mean square pressure perturbation
r	distance from source to observer
$\hat{r}$	unit normal vector from source to observer

ret retarded (source) time
SPL Sound Pressure Level (dB)
T_{ij} Lighthill stress tensor
t observer time
U_∞ freestream velocity
U_i refer to equation 2
u_i ith fluid velocity component
v_i ith surface velocity component of integration surface f = 0•- 3 -
x observer location vector
$\delta(f)$ Dirac delta function
ρ density
ρ_0 free-stream density
τ retarded time
$\Box^2$ wave operator $1/c^2\ \partial^2/\partial t^2 - \nabla^2$

INTRODUCTION

The Ffowcs Williams-Hawkings (FW-H) equation has recently been used with permeable surfaces in order to predict aerodynamic noise[1,2]. It is an inexpensive method to include the quadrupole source terms inside the FW-H surface without performing any volume integrations. This can significantly improve the accuracy of the noise predictions at locations where nonlinear interactions in the flow cannot be ignored. This is notably the case with highly turbulent flows such as high Reynolds number jets and wakes. It is also only slightly more expensive to use than a moving Kirchhoff surface (see Özyörük and Long[3]), but without the limitations of Kirchhoff methods.

The motivation for predicting the far-field noise generated by a 4-wheel landing gear stems from the increasing contribution of airframe noise to the overall sound level of an aircraft in its landing approach. Early studies in the 1970's by Heller and Dobrzynski[4] showed that high-lift devices such as slats and flaps, as well as deployed gears, generated noise levels 10 dB higher than those of an aircraft in its "clean" cruise configuration. Aerospatiale (now EADS Airbus) investigated the noise produced by several Airbus airplanes, which seems to indicate that noise from high-lift devices is likely to dominate for medium size aircraft, while landing gear noise seems more of a problem for existing and future high capacity aircraft. The importance of investigating landing gear noise is reinforced by Airbus Industry plans to extend the Airbus family towards a high capacity aircraft.

Heller and Dobrzynski carried out a series of tests with both scale models[4] and full scale models[5], which underscored the lack of detailed geometric features with model-scale experiments and their effects on high frequency noise. These early experiments also showed that there is an increase in noise radiation from tandem axle configurations, which is the second test case in the present study. However, it was also found during the full scale experiment that struts, braces and other small features contribute significantly to the overall sound level. A more recent work by Dobrzynski et al[6], where the impact of various gear sizes and configurations is measured, illustrates the difficulty in using scale-model results for full-scale noise predictions. The actual simulation of the landing gear flow field is also of interest since it potentially affects the inflow of flaps located

downstream. This was experimentally shown by Stoker et al[7] during a wind tunnel investigation of the airframe noise radiated by a model-scale Boeing 777, in which case a second high-frequency noise source from the flap system is only seen in the presence of the landing gear. This landing gear – flap interaction noise source was even shown to increase significantly by using a highly detailed gear geometry.

As already performed in a previous study by the same authors[8], the goal here is to combine the flexibility of unstructured grids with the FW-H equation. This is a unique combination of low-order unstructured grid solver methods with the well-proven FW-H equation, allowing for the aerodynamic and aeroacoustic investigation of landing gear geometries much more complex than those studied so far using structured grid CFD codes. The long-term objective is to model landing gear and other airframe components of increased fidelity in order to assess the impact of all small features, with the only limitation being that of computing power. We use the Parallel Unstructured Maritime Aerodynamics (PUMA) code for generating the flow data. PUMA has been validated in several instances for simulating time-accurate flow data[9,10]. The aim in the present case is to evaluate the impact on the noise directivity and intensity of two landing gear geometries (LDG1 and LDG2). It is expected to observe larger pressure fluctuations and a more complex three-dimensional flow in the case involving two additional struts (LDG2).

The Computational Grids

The grids used for the simulation of the flow over both landing gear configurations were generated using the commercial package Gridgen by Pointwise, Inc. Figure 1 and Figure 2 show an overall view of the meshes on the landing gear surfaces without and with lateral struts respectively. The first mesh consists of about 80,000 surface triangles, for a total of about 880,000 tetrahedra in the volume mesh. The second mesh reused as much of the previous grid features as possible. With two additional struts, the number of triangles on the surface went up to 135,000, with about 1.2 million tetrahedral cells. Specific attention was given to the cell clustering between the front and rear wheels, in order to capture as much of the wake from the upstream wheel impinging on the downstream wheel. Flow separation from the fore wheel and wake impingement on the aft are expected to generate large unsteady pressure fluctuations and therefore noise. With the second geometry, great care was given to the mesh refinement between the two lateral struts, with the aft strut in the wake of the fore strut. The smallest geometric features were not overly simplified, since they have been shown to generate high frequency noise as explained in a later section describing the Ffowcs Williams – Hawkings equation. This geometry was chosen because there are plans to run this same configuration in a wind tunnel and in a numerical experiment using the structured grid solver CFL3D with as many as 13.5 million grid points. Some of the smallest features are not included in this simulation in order to match other on-going tests at NASA Langley who provided the authors with the landing gear geometry: however, the use of state-of-the-art unstructured mesh generators will make this approach a valid tool for the investigation of complete landing gear configurations including hydraulic lines and braces in the future. The current simulations represent a

significant step towards realistic landing gear simulations when compared to some of the recent landing gear geometries investigated experimentally by Lazos[11] or using an incompressible Detached Eddy Simulation by Spalart[12].

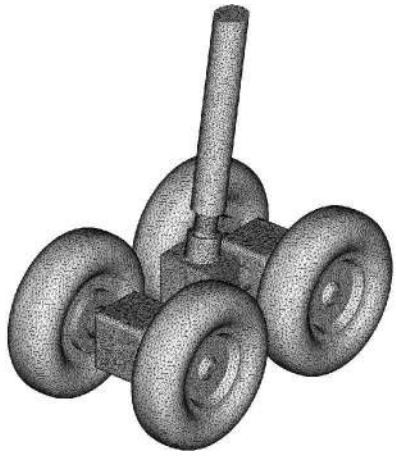

Figure 1. Surface mesh of first landing gear configuration (LDG1)

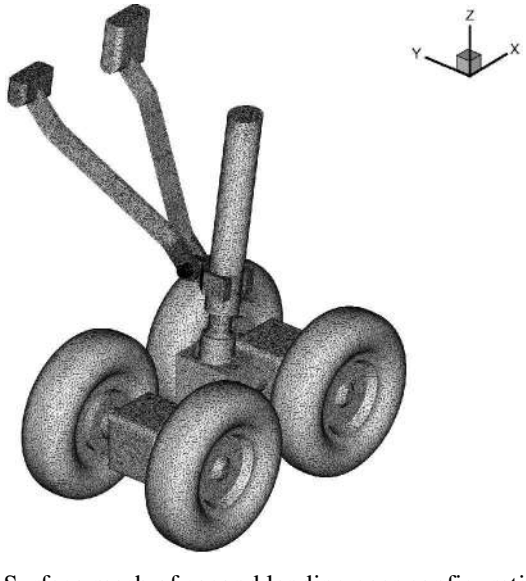

Figure 2. Surface mesh of second landing gear configuration (LDG2)

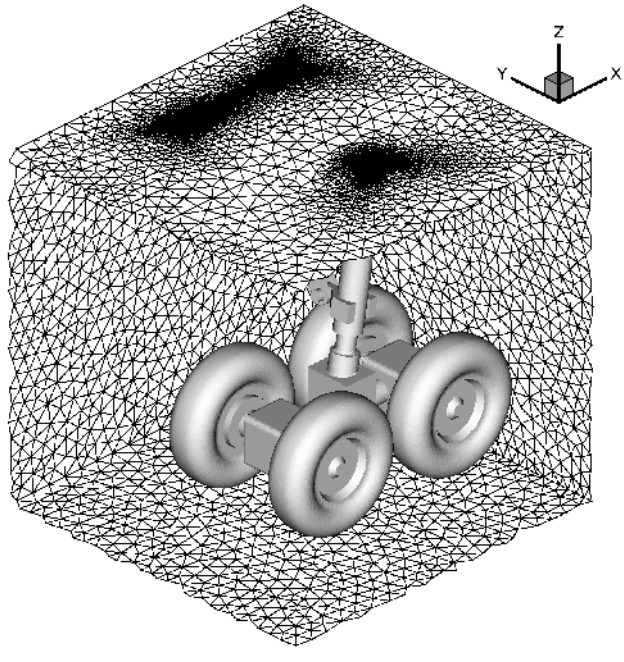

Figure 3. Partial view of the porous FW-H surface around LDG2 gear configuration

As shown in Figure 3 for the second geometry (LDG2), a porous FW-H integration surface was used in addition to the flow data collected on the landing gear surfaces themselves. This helps to determine the magnitude of the quadrupole source term for this low Mach number flow. Permeable FW-H surfaces were used for both geometries, with about 13,000 triangles in the first case, and 15,500 triangles in the case including two lateral struts. This coarsening mesh away from the solid surface is due to computer limitations. It may not be able to support the higher frequency pressure fluctuations. The advantage of these porous surfaces is that they can capture quadrupole-like terms without having to perform any volume integration. FW-H surfaces can be used in regions dominated by nonlinear effects (unlike the Kirchhoff formulations).

The Gibbs-Poole-Stockmeyer algorithm[13] was used to speed-up the communication process between CPUs. As shown in Figure 4, this procedure divides the domain into slices that minimize the number of messages between each processor, so that each CPU exchanges data with at most two neighboring CPUs. The time step for the unsteady simulations is determined by the smallest cell characteristic length. At a CFL number of 0.95, this yields a time step of 0.86E-08 second for the first grid, and 1.90E-08 second for the second grid (due mostly to some improved CAD work in the original geometry file). The numerical conditions were dictated by the CFL3D run performed at Langley: the Reynolds number based on the wheel diameter is 1.25 million, for a free stream Mach number of 0.2. The actual wheel diameter of the landing gear model is 9.4 cm.

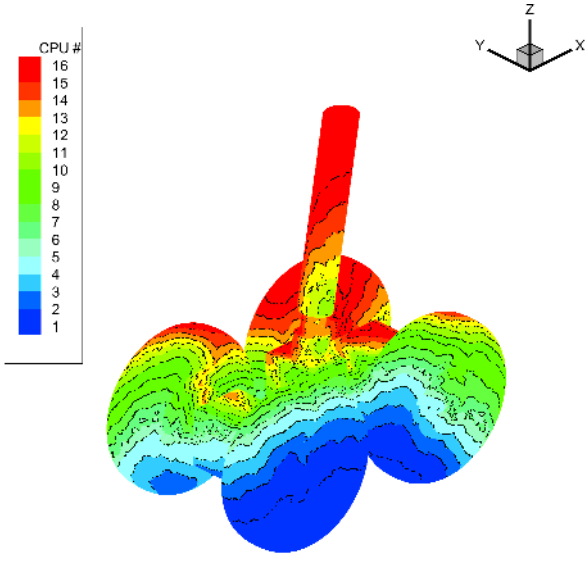

Figure 4. GPS partitioning on LDG1 landing gear surface across 16 processors

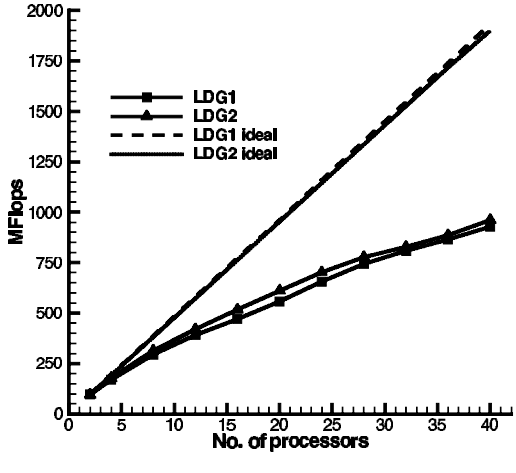

Figure 5. Parallel speed up on COCOA2 for both landing gear configurations

Flow Solver

PUMA (Parallel Unstructured Maritime Aerodynamics) is the computer program that was used to run the unsteady calculations. It is a finite volume, Runge-Kutta time-marching code that solves the compressible Navier-Stokes equations and uses unstructured grids. It uses the Message Passing Interface (MPI) library for parallel implementation. Its scaling performance for the two configurations is illustrated in Figure 5. The flop performance is slightly higher for the second case for any given

number of CPUs, since the ratio of computation over communication is greater for a larger grid. The facility used to perform the computation is the latest our two Cost effective Computing Arrays (COCOA and COCOA2)[14]. COCOA2 is a Beowulf cluster comprised of 20 nodes each having dual 800 MHz Pentium III and 1 GB RAM. The cluster has dual fast-Ethernet on each node and all the nodes are connected using two HP2524 switches with channel bonding for increased data communication. These machines run Redhat Linux (version 7.0) and the gcc compiler.

For these simulations the inherent artificial dissipation provided by Roe's flux integration scheme acts as a sub-grid scale turbulence model. A parallel investigation on separated flow around a cone[15] shows that the implementation of a Large Eddy Simulation (LES) method using a Smagorinsky sub-grid scale model[16] may improve PUMA's ability to simulate both mean and turbulent quantities in the wake of a cone base flow. LES has already been used extensively to compute sound sources[17,18], but some recent work related to two-time statistics of LES data, would indicate that LES fields are too coherent if the eddy viscosity model does not include any random backscatter[19]. One way to circumvent this may be the use of a dynamic LES, which is more likely to yield enough backscattering to decorrelate the fluid motion at large scales. An example of the use of a dynamic subgrid scale model combined with a Ffowcs Williams – Hawkings solver is given by Morris et al[20] in an attempt to simulate the jet noise for circular nozzles.

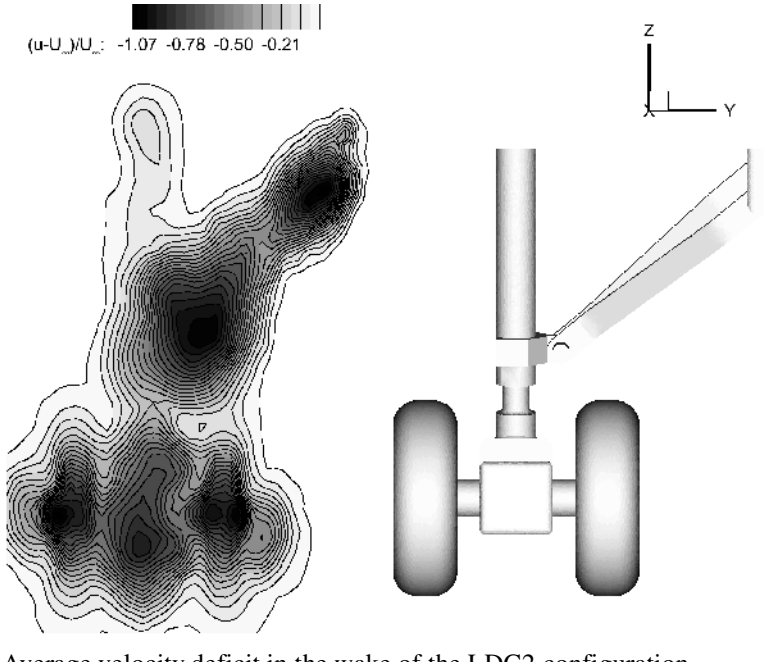

Figure 6. Average velocity deficit in the wake of the LDG2 configuration

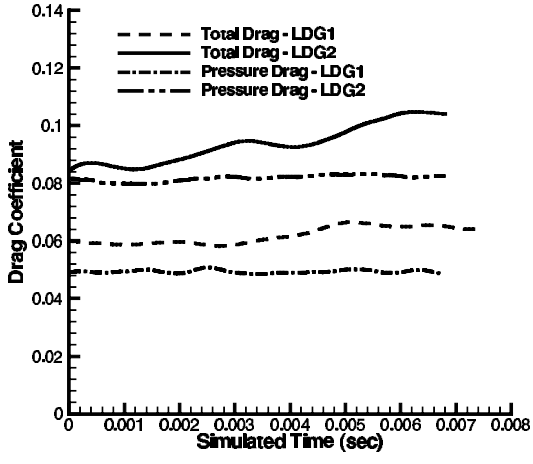

Figure 7. Time-history of drag force coefficients for landing gear configurations LDG1 and LDG2 using pressure and wake methods

SIMULATION RESULTS

Simulations were carried out over two cycles based on the expected shedding frequency based on the wheel diameter. Each simulation took about 90 days on 24 CPUs. It is worth mentioning that the existing amount of data for both gear configurations put a strain on the available capacity in terms of storage requirements: about 40 Gigabytes of data have been collected for the two calculations described in this study. Data were sampled only for the second cycle to minimize the effects of the starting conditions. Local time stepping was initially used to accelerate the convergence from free-stream conditions to a realistic state. This is achieved by assigning to each cell the maximum allowable time step for a given CFL number (pseudo time marching). Global time stepping is then turned on before unsteady data is sampled. In order to evaluate the total drag, the momentum deficit method is used by evaluating the velocity deficit in the wake of the landing gear. More details can be found in Rae and Pope[21]. The pressure based method and the wake deficit approach have been used successfully with PUMA for complex flow simulations such as that of a Bell 214 ST fuselage at similar Reynolds numbers[15,22]. The pressure drag predictions were within 5% of the measured drag. During the same investigation, very good agreement was obtained for the pressure distribution on the helicopter surface, even where the flow experienced massive separation phenomena. PUMA's ability to predict wake data with accuracy was also tested for the turbulent wake past a cone[8] and it too was predicted well. Figure 6 shows the average velocity deficit right behind the second gear configuration. In the second gear case, there is a good qualitative agreement with experimental results published by Stoker[7] in the high-fidelity landing gear configuration. Figure 7 shows the drag forces computed by integrating the pressure on the gear surface (pressure drag) and using Pope's wake deficit approach (labeled total drag). Results are shown for both gear configurations during approximately 7 milliseconds of simulated flow time, giving enough time for the fluid to cover three times the gear total length. The

force coefficients (drag, lateral and vertical force) are the computed forces divided by the landing gear surface area and the dynamic pressure. The increase in overall drag due to the introduction of the lateral support struts is large since these components are not aerodynamically profiled and are comparable to flat plates facing the incoming fluid flow. Figure 8 illustrates the lateral forces stemming from the presence of these two struts.

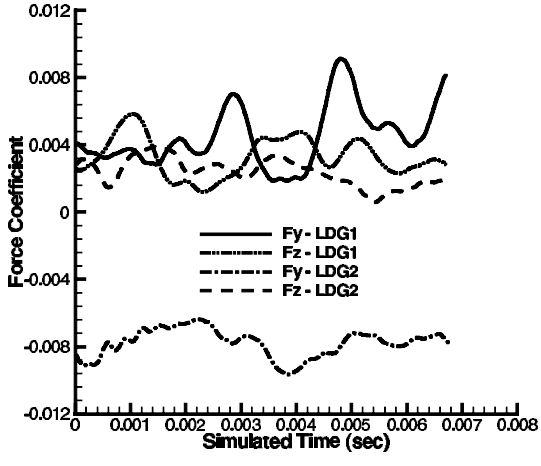

Figure 8. Time-history of lateral (Fy) and vertical (Fz) pressure force coefficients for configurations LDG1 and LDG2

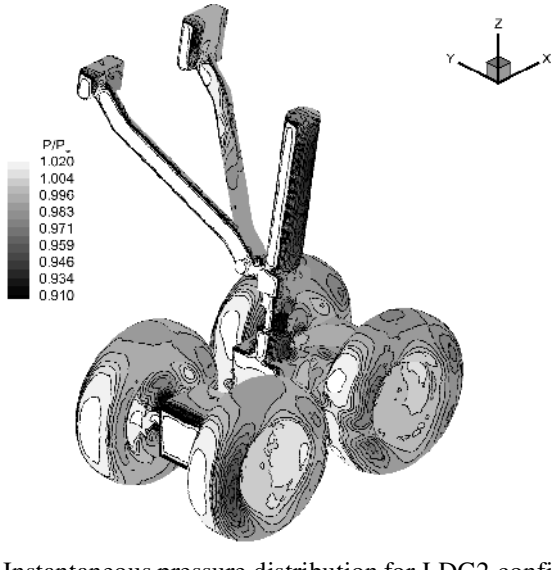

Figure 9. Instantaneous pressure distribution for LDG2 configuration

One expects the far-field sound pressure level to reflect this unsteady loading in both its intensity and directivity. Figure 9, which is a display of the instantaneous distribution of pressure on the landing gear surface in its second configuration, shows the pressure on these support struts, as well as on the wheels. Figure 10 shows a 3D representation of some vortex filaments shedding off various gear components, and highlight the impact of the upstream elements' wake onto gear elements at downstream locations. The effect of these vortices is not completely captured by the FW-H surface which lies on the landing gear itself. However the permeable FW-H surface does account for all the effects induced by these filaments until they cross its boundaries.

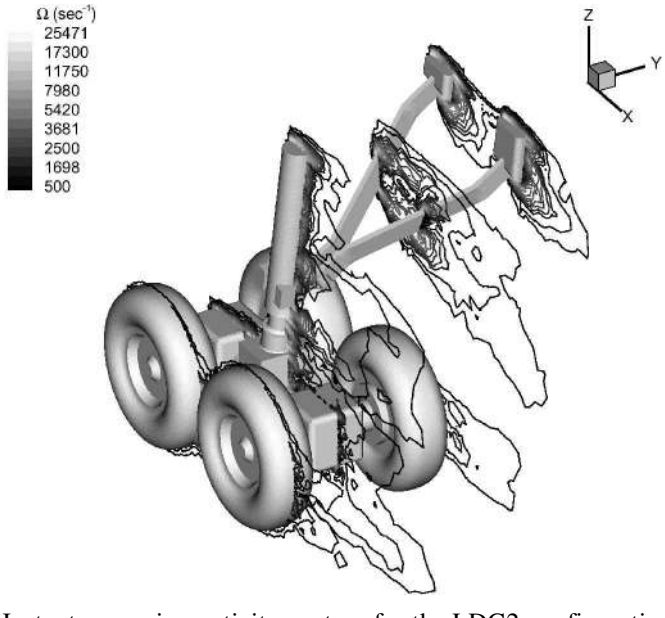

Figure 10. Instantaneous isovorticity contour for the LDG2 configuration

FAR-FIELD NOISE PREDICTION

Only recently has the FW-H equation been used on a permeable surface. di Francescantonio[23] was able to show that simply integrating the surface source terms on a porous FW-H surface does account for the quadrupole sources enclosed within the surface. The FW-H equation is written in the standard differential form including all quadrupole, dipole and monopole source terms as

$$\Box^2 \rho'(\mathbf{x}, t) = \frac{\partial^2}{\partial x_i \partial x_j}[T_{ij} H(f)] - \frac{\partial}{\partial x_i}[L_i \delta(f)] + \frac{\partial}{\partial t}[(\rho_0 U_n)\delta(f)] \qquad [1]$$

where L_i and U_n are defined as

$$U_n = U_i \hat{n}_i \qquad U_i = \left(1 - \frac{\rho}{\rho_0}\right) v_i + \frac{\rho u_i}{\rho_0}$$

$$L_i = P_{ij} \hat{n}_j + \rho u_i (u_n - v_n) \qquad [2]$$

The subscript n indicates the projection of a vector quantity in the surface normal direction. Using the solution to the above equation given in Brentner and Farassat[24] and neglecting the quadrupole terms, the pressure fluctuation at a given observer location **x** and time t is (equation 3 below)

$$4\pi p'(\mathbf{x}, t) = \int_{f=0} \left\{ \left[\frac{\rho_0 \dot{U}_n}{r (1 - M_r)^2} \right] + \left[\frac{\rho_0 U_n c (M_r - M^2)}{r^2 (1 - M_r^3)} \right] \right\}_{ret} dS$$
$$+ \qquad [3]$$
$$\int_{f=0} \left\{ \frac{1}{c} \left[\frac{\dot{L}_r}{r (1 - M_r)^2} \right] + \left[\frac{L_r - L_M}{r^2 (1 - M_r)^2} \right] + \left[\frac{L_r (M_r - M^2)}{r^2 (1 - M_r)^2} \right] \right\}_{ret} dS$$

FW-H code validation

In the absence (at the moment) of experimental acoustic data to compare to, an already-proven method was implemented: the use of the CFD results to validate the FW-H sound predictions. As was done by the authors in a previous test case[8], the pressure fluctuations computed by the flow solver PUMA at an observer in the near field were compared with the predictions given by the FW-H post-processing utility. Although the near-field pressure fluctuations are large, and likely contain a great amount of hydrodynamic oscillations, the derivation of the FW-H equation is such that all pressure perturbations (acoustic and hydrodynamic) should be recovered. Examples in the near field are given by Farassat and Brentner[25] in the case of high-speed impulsive noise at rotor blade tip Mach number close to 0.9. It is assumed that at a Mach number of 0.2, the quadrupole terms do not contribute significantly to the far-field noise. The solution p'_Q to the quadrupole term of the FW-H equation is:

$$4\pi p'_Q(\mathbf{x}, t) = \frac{\partial^2}{\partial x_i \partial x_j} \int_{-\infty}^{t} \int_{f>0} \frac{T_{ij}}{r} c \, d\Omega d\tau \qquad [4]$$

The volume integration, if performed, must be carried out over a large volume and represents a large computational task. The far field approximation of equation 4 reduces to:

$$4\pi p'_Q(\mathbf{x}, t) = \frac{1}{c} \frac{\partial^2}{\partial t^2} \int_{-\infty}^{t} \int_{f>0} \frac{T_{rr}}{r} d\Omega d\tau \qquad [5]$$

However, there is in the present case an interest in capturing quadrupole effects in the near field, so that an exact result to the FW-H equation is needed instead of the far field approximation. Farassat and Brentner[26] decomposed the quadrupole noise term into three components varying with *1/r*, *1/r²* and *1/r³* respectively:

$$4\pi p'_Q(\mathbf{x}, t) = \frac{1}{c}\frac{\partial^2}{\partial t^2}\int_{-\infty}^{t}\int_{f>0}\frac{T_{rr}}{r}\,d\Omega d\tau + \frac{\partial}{\partial t}\int_{-\infty}^{'}\int_{f>0}\frac{3T_{rr}-T_{ii}}{r^2}\,d\Omega d\tau + c\int_{-\infty}^{'}\int_{f>0}\frac{3T_{rr}-T_{ii}}{r^3}\,d\Omega d\tau$$

There is a possibility that the second and third terms may contribute in a significant way to the near field pressure variations. This implies that in order to validate the FW-H predictions against the CFD results one may have to account for some of these nonlinear effects in addition to loading noise in the near field since the observer is in a highly perturbed propagating medium. In the current derivation of the FW-H equation, the quadrupole term is not computed (to reduce computing time and to limit storage requirements). However the porous FW-H surface shown in a previous figure has the ability to recover all nonlinear effects occurring within its own boundaries. Figure 11 is an illustration of the instantaneous pressure distribution on the permeable FW-H integration surface.

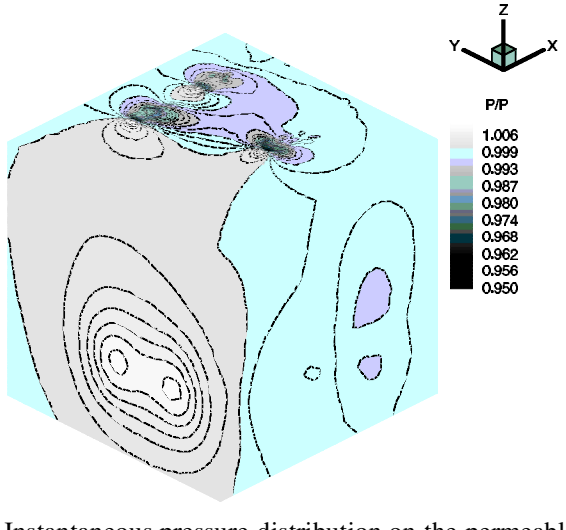

Figure 11. Instantaneous pressure distribution on the permeable FW-H surface for the LDG2 configuration

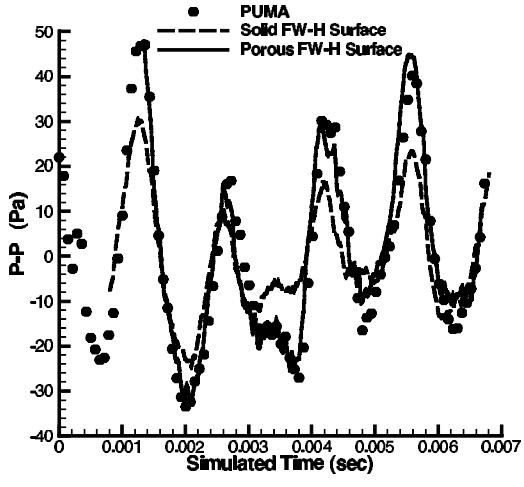

Figure 12. Comparison in the near-field of the FW-H predictions from integration surfaces 1 and 2 versus the PUMA solver results

Observers were placed just above the landing gear main leg ($x = 2.68$ cm, $y = 0$ cm and $z = 17$ cm for observer whose pressure is depicted in Figure 12), where the porous FW-H mesh is more refined, so that the FW-H predictions can take place using both the solid and the porous FW-H surfaces. An example of comparisons with the PUMA results at one of these near-field observer locations is shown in Figure 12. This shows good agreement between the porous FW-H surface predictions and the solver computation, whereas the solid FW-H surface misses by more than 50% some of the pressure fluctuations. This demonstrates the ability of the second FW-H surface to predict the entire pressure oscillations, either of acoustic or hydrodynamic nature. It tends to suggest that quadrupole effects may represent a significant contribution to the overall near-field sound level and hydrodynamic fluctuations even at moderate Mach numbers. Unless a volume integration is performed over the entire CFD domain, the entire pressure perturbation cannot be exactly reproduced where nonlinear effects are important and where vortices flow across the permeable FW-H surface. Fast Fourier Transforms (FFT's) were applied to the pressure predictions from both surfaces as well as to the pressure signal sampled from the PUMA solver and are shown in Figure 13. The sampling time and frequency for the FW-H pressure predictions were different than that of the PUMA solver. This is reflected in slight shifts in the lowest and highest frequency data. The horizontal axis represents the Strouhal number based on the landing gear main leg diameter. The main peak is observed at a Strouhal number just above 0.2. The observer is located right in the wake of the main gear leg, so that the signal is driven by the shape and dimension of this leg. This Strouhal number value corresponds to the range of measured and simulated Strouhal numbers from state-of-the-art Large Eddy Simulations for similar Reynolds numbers listed by Wang[27], for rough cylinder surfaces, which is the case when taking into account the discretization of the cylinder surface and numerical errors.

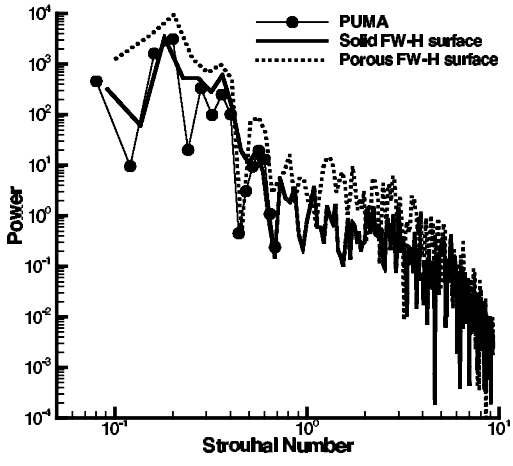

Figure 13. Power spectral density from Fast Fourier Transforms applied to solid and porous FW-H surface predictions and PUMA solver results

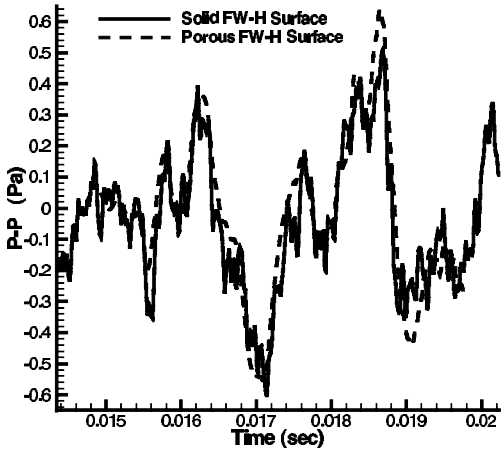

Figure 14. Comparison of the FW-H far-field predictions from solid and porous integration surfaces at 40 wheel radii and 50° angle from downstream axis

As expected, the agreement between the predictions from the two FW-H surfaces improves in the far-field. Figure 14 shows the pressure time history at 40 radii from the landing gear at a 50 degree angle with respect to the downstream axis. The field produced by the coarser FW-H surface off the landing gear does not reflect the same high-frequency fluctuations given by the predictions coming from data collected on the gear itself. In view of experimental results described earlier, it was decided to use the solid FW-H surface to investigate the far-field noise directivity, where high-frequency signals are thought to be significant. Figure 15 below illustrates the decrease of the RMS pressure

signal as one moves away from the landing gear along the downstream axis. Calculations were made at 20 observers from 25 to 50 wheel diameters in the wake of the landing gear. Both FW-H surface data were used and compared with a trend line assuming a signal decaying with *1/r*. As observed previously, the agreement between the two surface predictions improves with increasing distance from the landing gear. As one moves further away from the landing gear, it is seen by the observer as an acoustic compact source, and the signal intensity should decrease with the inverse of the distance from the source. There is a change of slope as one moves closer to the landing gear, reflecting the impact of source terms whose dependence is a higher power of *1/r*.

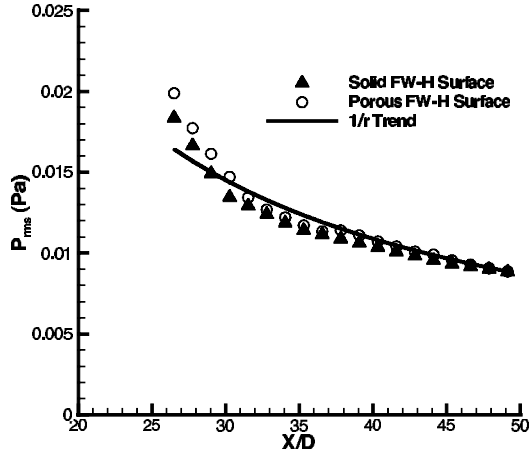

Figure 15. RMS pressure signal predictions from solid and porous FW-H integration

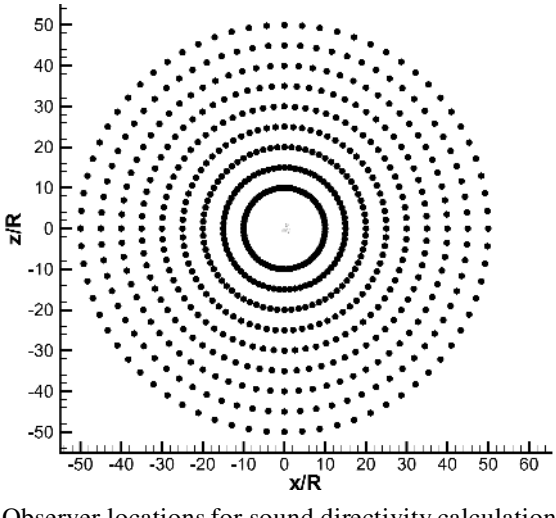

Figure 16. Observer locations for sound directivity calculations

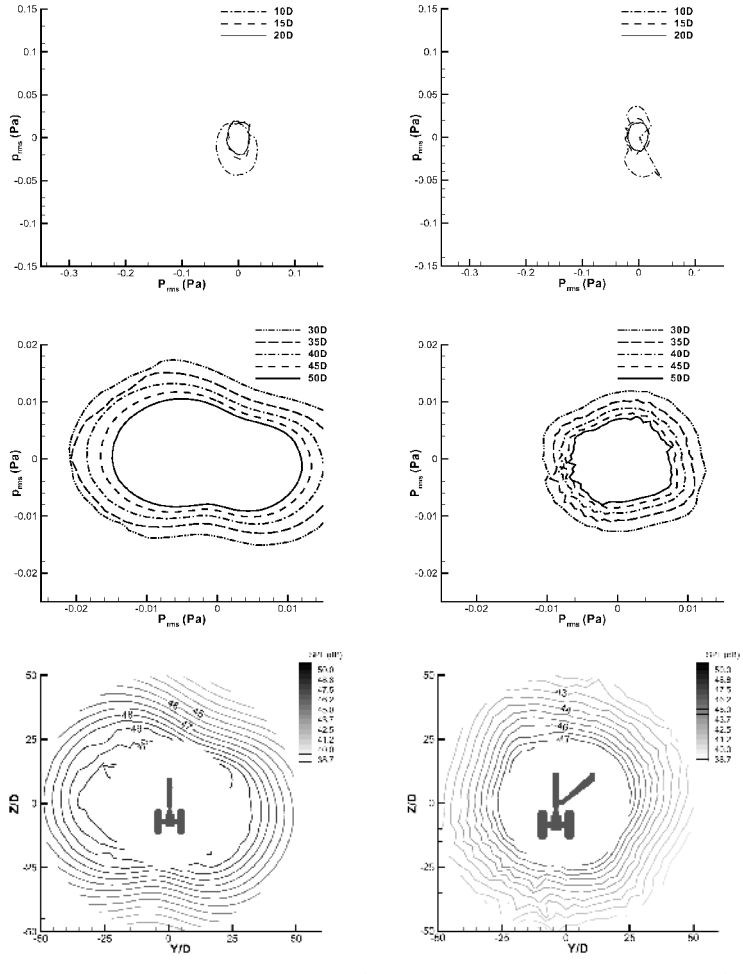

Figure 17. Medium-field RMS pressure (top), far-field RMS pressure (middle) and SPL contour (bottom) from streamwise perspective for LDG1 (left) and LDG2 (right)

Sound directivity patterns

The sound directivity in the medium- and far-field requires the use of a parallel version of the FW-H post-processing program[8,28]. For each radii away from the landing gear, 72 observer locations are defined, so that a resolution of 5 degree angle is obtained. A total of 648 observer points were defined, and are illustrated in Figure 16, which shows the relative scale with respect to the landing gear. For both gear configurations, all three orientation planes were studied and the results are reported in Figures 17a to 17f, Figures 18a to 18f and Figures 19a to 19f for the first and second gear configurations from a streamwise, spanwise and vertical perpective respectively. Polar directivity

plots at radial locations of 10, 15 and 20 radii from the gear are plotted separately from the locations further away (30 to 50 radii from the gear) for scaling issues. Sound Pressure Level (SPL) contours with a reference pressure of 6×10^{-5} Pa are also presented for radial locations varying from 25 to 50 radii from the landing gear. The scale for equivalent configurations is unchanged in order to allow for qualitative comparisons with respect to both directivity and intensity of the sound pressure signal. In Figures 17 to 19, the landing gear is not to scale, and is meant to illustrate which orientation axis is shown. The low SPL values that are shown in these figures (from 40 to 50 dB) are a reminder of the landing gear's small dimensions and the resulting dipole dominated noise at low Mach numbers, which scales with the landing gear surface area.

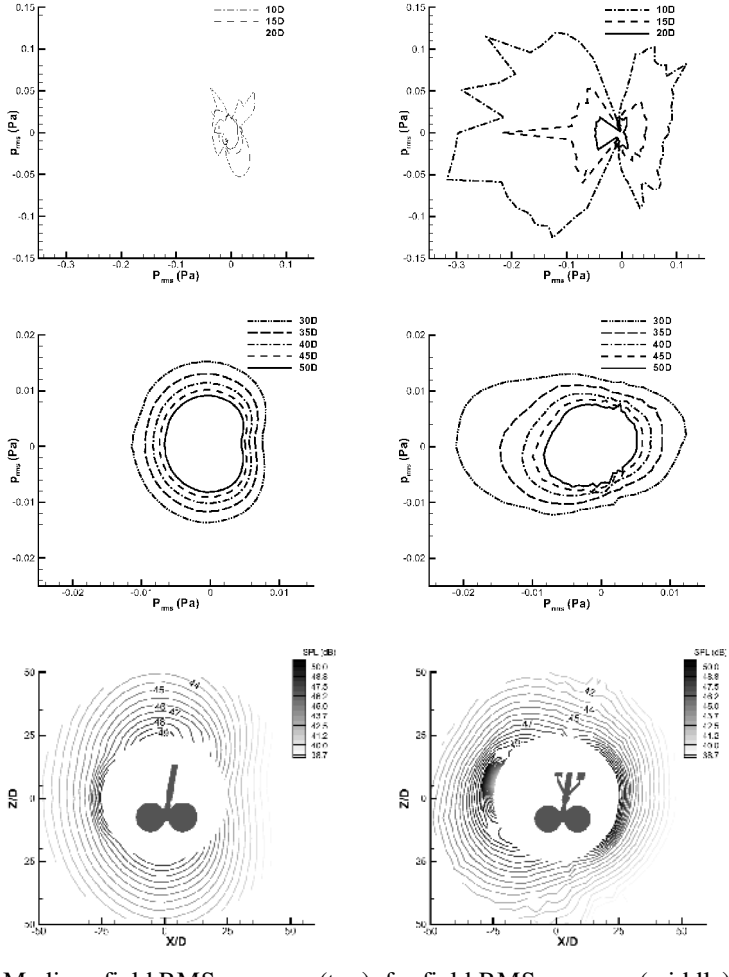

Figure 18. Medium-field RMS pressure (top), far-field RMS pressure (middle) and SPL contour (bottom) from sideways perspective for LDG1 (left) and LDG2 (right)

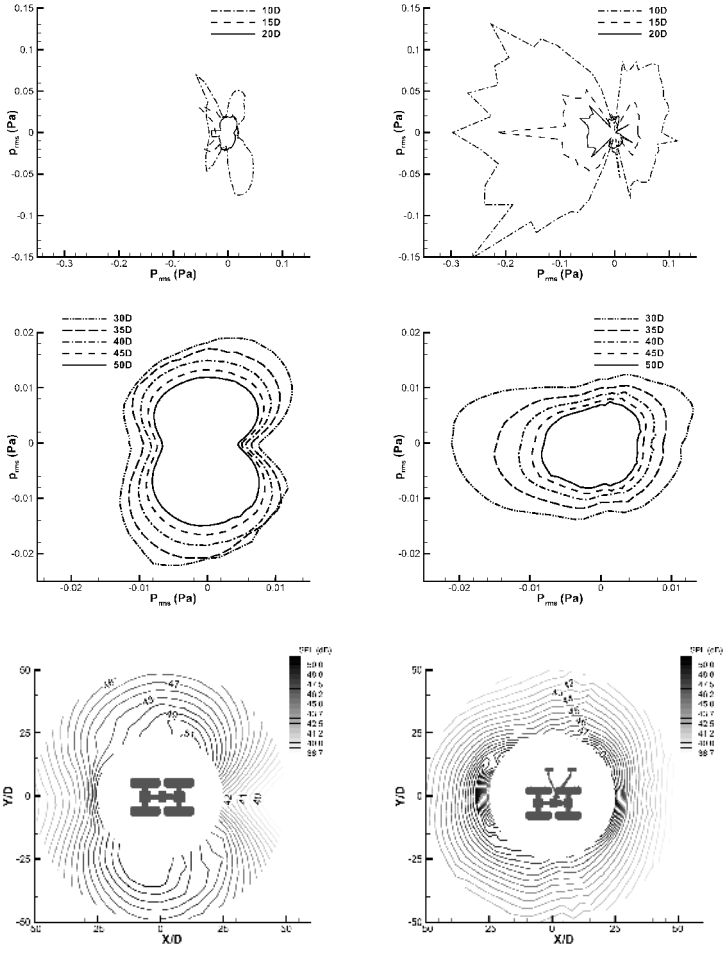

Figure 19. Medium-field RMS pressure (top), far-field RMS pressure (middle) and SPL contour (bottom) seen from above for LDG1 (left) and LDG2 (right)

The drag augmentation is reflected in the sound directivity patterns of both configurations. The intensity of the RMS pressure is greatly increased along the streamwise direction for the second gear case (LDG2). This is due to the two support struts on the aerodynamic profile of the landing gear. Regarding the lateral noise, the two struts seem to interfere with the build-up of sound, so that the signal in the spanwise direction is less than that in the clean configuration, where varying lateral forces on the gear leg create pressure levels in the far-field comparable to those along the streamwise direction. In both cases, the near-field pressure perturbations are dominated by the fluctuations in drag. Little noise is generated in the vertical direction since most of the lift and drag variations are generated on the main gear leg. The overall

pressure field looks much more disturbed in the second gear configuration, illustrating the complex three-dimensionality of the noise-generating flow pattern.

CONCLUSION

The flow field around two landing gear configurations of increasing complexity has been assessed. The wake deficit observed behind the landing gear is very similar to that experimentally measured on comparable configurations. A parallel version of the Ffowcs Williams – Hawkings equation has been implemented using inexpensive Beowulf clusters to extract near- and far-field sound information. Both solid and permeable FW-H integration surfaces have been used. Excellent agreement has been obtained in the near field between the porous FW-H surface predictions and the CFD solver results where hydrodynamic fluctuations are expected to dominate and are of greater magnitudes than those typical of acoustic signals. More work is needed in order to show that the discrepancy observed between the solid and porous FW-H surfaces in the near-field is linked to short-range quadrupole-like effects even though the problem that was dealt with in the present case is a relatively low Mach number flow for this kind of effects to be significant. The comparison of power spectra at the same near-field observer illustrates the quality of this low-order flow simulation compared to other numerical and wind tunnel experiments for shapes similar to that of the landing gear components. It also shows a good agreement between the frequency content of both FW-H predictions with that of the flow solver.

The comparison of acoustic predictions produced by the two FW-H surfaces improves as the observer location is moved further away in the far field. The increase in drag stemming from the lateral struts is reflected in the noise level and directivity. There is a significant increase in sound intensity in the streamwise direction, whereas the disturbance caused by these gear elements seems to interfere with the vortex shedding off the gear leg and the resulting lateral sound radiation.

ACKNOWLEDGMENTS

Support provided by NASA Langley Research Center through grant NAG 1-2147 and the National Science Foundation through grant EIA-99-77526 is gratefully acknowledged.

REFERENCES

1. Singer, B. A., Brentner, K. S., Lockard, D. P. and Lilley, G. M., (1999) *Simulation of Acoustic Scattering from a Trailing Edge*, AIAA Paper 1999-0231, 37 th Aerospace Sciences Meeting and Exhibit, Reno, NV.
2. Singer, B. A., Lockard, D. P., Brentner, K. S., Khorrami, M. R., Berkman, M. E. and Choudhari, M., (1999) *Computational Aeroacoustic Analysis of Slat Trailing-Edge Flow*, AIAA Paper 1999-1802, 5th AIAA/CEAS Aeroacoustics Conference, Greater Seattle, WA.
3. Özyörük, Y. and Long, L. N., A New Efficient Algorithm for Computational Aeroacoustics on Parallel Processors, *Journal of Computational Physics*, Vol. 125, pp. 135-149.

4. Heller, H. H. and Dobrzynski, W. M., (1977) Sound Radiation From Aircraft Wheel-Well/Landing-Gear Configurations, *J Aircraft*, Vol. 14, No. 8, Aug. 1977, pp. 768-774.
5. Dobrzynski, W. M. and Buchholz, H., *Full-Scale Noise Testing on Airbus Landing Gears in the German Dutch Wind Tunnel*, AIAA Paper 97-1597.
6. Dobrzynski, W., Chow, L. C., Guion P. and Shiells, D., (2000) *A European Study On Landing Gear Airframe Noise Sources*, AIAA Paper 2000-1971, 6th AIAA/CEAS Aeroacoustics Conference and Exhibit, Lahaina, HI.
7. Stoker, R. W. and Sen, R., (2001) *An Experimental Investigation of Airframe Noise Using a Model-Scale Boing 777*, AIAA Paper 2001-0987, 39th Aerospace Sciences Meeting and Exhibit, Reno, NV.
8. Long, L. N., Souliez, F. and Sharma, A., (2001) *Aerodynamic Noise Prediction Using Parallel Methods on Unstructured Grids*, AIAA Paper 2001-2196, 7th AIAA/CEAS Aeroacoustics Conference, Maastricht, The Netherlands.
9. Modi, A. and Long, L. N., (2000) *Unsteady Separated Flow Simulations using a Cluster of Workstations*, AIAA Paper 2000-0272, 38th Aerospace Sciences Meeting and Exhibit", Reno, NV.
10. Sharma, A. and Long, L. N., (2001) *Airwake Simulations on LPD17 Ship*, AIAA Paper 2001-2589, 31st AIAA Fluid Dynamics Conference and Exhibit, Anaheim, CA, 2001.
11. Lazos, B. S., (2002) Mean Flow Features Around the Inline Wheels of Four-Wheel Landing Gear, *AIAA Journal*, Vol. 40, No. 2, Feb. 2002, pp. 193-198.
12. Hedges, L. S., Travin, A. and Spalart, P. R., Detached-Eddy Simulations over a Simplified Landing Gear, to appear in *Journal of Fluids Engineering.*
13. Duff, I. S., Erisman, A. M. and Reid, J. K., *Direct Methods for Sparse Matrices*, Oxford University Press, 1986.
14. Long, L. N. and Modi, A., (2001) *Turbulent Flow and Aeroacoustics Simulations using a Cluster of Workstations*, Linux Revolution Conference, Champaign, IL, June 2001.
15. Souliez, F. J., (2002) *Parallel Methods for Computing Unsteady Separated Flows Around Complex Geometries*, PhD thesis, Penn State University.
16. Smagorinsky, J., (1963) General Circulation Experiments With the Primitive Equations, *Monthly Weather Review*, No. 91, pp. 99-165.
17. Piomelli, U., (1999) Large-Eddy Simulation: Achievements and Challenges, *Progress in Aerospace Sciences*, Vol. 35, pp. 335-362.
18. Seror, C., Sagaut, P., Bailly, C. and Juve, D., (2001) On the Radiated Noise Computed by Large-Eddy Simulation, *Phys. Fluids,* Vol. 13, pp. 476-487.
19. He, G., Rubinstein, R. and Wang, L. P., *Effects of Eddy Viscosity on Time Correlations in Large Eddy Simulation*, ICASE Report No. 2001-10.
20. Morris, P. J., Scheidegger, T. E. and Long. L. N., (2000) *Jet Noise Simulations for Circular Nozzles*, AIAA Paper 2000-2080, 6th AIAA/CEAS Aeroacoustics Conference and Exhibit, Lahaina, HI.

21. Rae, W. H. and Pope, A., (1984) *Low-Speed Wind Tunnel Testing*, second edition, Wiley-Interscience.
22. Souliez, F. J. and Long, L. N., Steady and Unsteady Flow Simulations Around a Bell 214ST Fuselage Using Unstructured Grids, submitted to the *Journal of the American Helicopter Society.*
23. di Francescantonio, P., (1997) A New Boundary Integral Formulation for the Prediction of Sound Radiation, *Journal of Sound and Vibration*, Vol. 202, No. 4, pp. 491-509.
24. Brentner, K. S., and Farassat, F., (1998) An Analytical Comparison of the Acoustic Analogy and Kirchhoff Formulation for Moving Surfaces, *AIAA Journal*, Vol. 36, No .8, Aug. 1998, pp. 1379-1386.
25. Farassat, F. and Brentner, K. S., (1998) Supersonic Quadrupole Noise Theory for High-Speed Helicopter Rotors, *Journal of Sound and Vibration,* Vol. 218, No. 3, pp. 481-500.
26. Farassat, F. and Brentner, K. S., (1988) The Uses and Abuses of the Acoustic Analogy in Helicopter Rotor Noise Prediction, *Journal of the American Helicopter Society*, Vol. 33, pp. 29-36.
27. Wang, M., Catalano, P. and Iaccarino, G., (2001) Predictions of High Reynolds Number Flow Over a Circular Cylinder Using LES with Wall Modeling, Stanford Center for Turbulence Research, *Annual Research Briefs 2001*, pp. 45-50.
28. Long, L. N. and Brentner, K. S., (2000) *Self-Scheduling Parallel Methods for Multiple Serial Codes with Application to WOPWOP*, Paper 2000-0346, 38th Aerospace Sciences Meeting and Exhibit, Reno, NV.